Journal of Magnetic Resonance **155,** 57–63 (2002)
doi:10.1006/jmre.2002.2512, available online at http://www.idealibrary.com on IDEAL®

Low-Symmetry Spin Hamiltonian and Crystal Field Tensors Analysis: Fe^{3+} in Natrolite

V. M. Vinokurov,* J. M. Gaite,† G. R. Bulka,* N. M. Khasanova,*,‡ N. M. Nizamutdinov,* A. A. Galeev,*,‡ and C. Rudowicz‡

*Kazan State University, Kremlevskaya str. 18, Kazan 420008, Russia; †Université d'Orleans, CNRS, Rue de Chartres, B.P. 6759, 45067 Orleans Cedex 2, France; and ‡Department of Phys. and Materials Science, City University of Hong Kong, Kowloon Tong, Hong Kong Special Administrative Region, China

Received July 26, 2001; revised December 21, 2001

Electron paramagnetic resonance study of a natural single crystal of natrolite was carried out at the frequency $\nu = 36.772$ GHz at room temperature. The angular dependence of the four symmetry-related spectra of Fe^{3+} in the three crystallographic planes was fitted to a spin Hamiltonian ($S = 5/2$) of symmetry C_i. The rank 4 crystal field tensors at tetrahedral sites were calculated using the point-charge model to determine the principal axes orientations of their cubic and trigonal components. The analysis of zero-field splitting tensors and comparison with crystal field ones suggests that Fe^{3+} substitutes for Al^{3+} with no significant distortion of the coordination tetrahedron in natrolite. Comparison of data for several natural and synthetic crystals reveals that the 4-rank zero-field splitting tensor invariants for Fe^{3+} at the tetrahedral oxygen-coordinated sites are distinguishably smaller than those for Fe^{3+} at octahedral sites. Such comparative analysis may help to determine the substitutional sites in other crystals.

Key Words: **natrolite; spin Hamiltonian; low symmetry effect; crystal field; tensor invariants.**

1. INTRODUCTION

Natrolite, $Na_2[Al_2Si_3O_{10}] \cdot 2H_2O$, space group C_{2v}^{19}—$Fdd2$ (*1*), is one of the fibrous zeolites with the framework constructed from the chains of corner-sharing Al and Si oxygen tetrahedra. The main structural unit is $Al_2Si_3O_{10}$ consisting of five tetrahedra, of which four are bound into the ring and the fifth, the SiO_4 tetrahedron, links the rings to form the chain extended along the *c*-axis (Fig. 1). The adjacent chains are connected by outer oxygen ions O2 of the rings, forming a three-dimensional framework. Ordered Na^+ ions and H_2O molecules fill the voids of the framework. By the use of a wide range of different methods including Raman spectroscopy and NMR in (*2*) it was found that the change in chemical composition of the nonframework ions and/or water content is followed by orientational changes (tilting and rotating) of the framework tetrahedra. The flexibility of the natrolite framework also allows partial disorder in (Al, Si) distribution (*3*). The presence of iron impurities in low concentration as usual traces in the natural crystals with natrolite type structure makes it possible to use electron paramagnetic resonance (EPR) technique for investigation of local field perturbations at the substitution sites in the framework caused by different modification of the structure.

The presence of Fe^{3+} impurity ions were established by EPR in natrolite at the K-band (*4*) and in scolecite $Ca[Al_2Si_3O_{10}] \cdot 3H_2O$ at the Q-band (*5*). In both cases the EPR spectra were described by the spin Hamiltonian (SH) of orthorhombic symmetry and the parameters were found from the measurements of the spectrum along the extreme points in the spectral angular dependence. A relatively large discrepancy was observed between the principal directions in the EPR spectra of these two crystals with natrolite type framework, which may result from: (i) difference in structural peculiarities of these two crystals; (ii) low-symmetry effects; (iii) difference in mechanisms of impurity ion substitutions for framework cations. It should be mentioned that some uncertainty can appear because of difference in procedures for distinguishing the spectrum principal directions in the case of their noncoincidence with symmetry elements of the crystals. In order to avoid this uncertainty and to determine the SH tensors of proper symmetry we studied the spectral angular dependence in the three symmetry planes of natrolite single crystal.

The main purpose of this work is to present and analyze the EPR results for Fe^{3+} ions in natrolite. In order to resolve the question of the Fe^{3+} substitution sites a topological analysis (i.e., pseudosymmetry (*6*)) of zero field splitting tensors (ZFS) in SH and crystal field (CF) tensors is performed and comparison of the rank 4 ZFS tensor invariants for the Fe^{3+} ions substituted for the 2-, 3-, and 4-valent host ions at tetrahedral sites is carried out using the EPR data on several compounds. Our work consists of the following steps: (1) detailed investigation of the angular dependence of the EPR spectra of Fe^{3+} in natrolite and fitting of the SH parameters; (2) analysis of both the ZFS tensor B_4 and the irreducible tensor product $[V_4 \otimes V_4]_4$ of the 4-rank CF tensor V_4 for Fe^{3+} at tetrahedral sites in natrolite; (3) calculation and comparison of the 4-rank ZFS invariants for Fe^{3+} at tetrahedral and octahedral sites; (4) study of the

1090-7807/02 $35.00

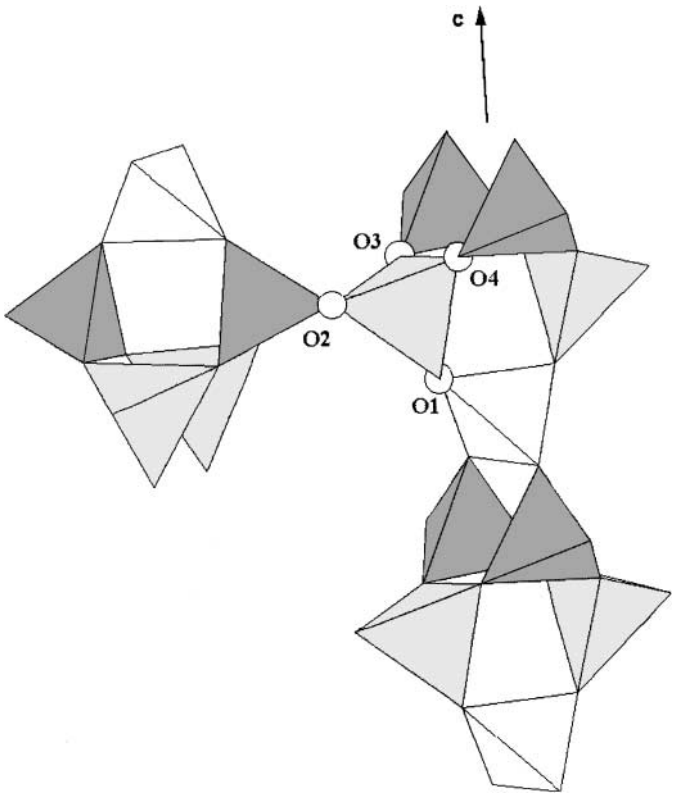

FIG. 1. Structural units of the natrolite framework. Si1 coordination tetrahedra—white, Si2 tetrahedra—dark, Al tetrahedra—light grey. Oxygen environment of Al is shown by circles.

possible orientations of the magnetic axes and the low-symmetry effects in the spectral angular dependence for Fe^{3+} in natrolite; (5) comparison with results on Fe^{3+} EPR in scolecite.

2. EPR OF Fe^{3+} IONS IN SINGLE CRYSTAL OF $Na_2[Al_2Si_3O_{10}] \cdot 2H_2O$

EPR of Fe^{3+} ions in natural natrolite single crystal was studied at the frequency $\nu = 36.772$ GHz at room temperature. As in (*4*), four conjugate spectra (i.e., spectrum multiplicity $K_M = 4$) were observed. In accordance with the space group C_{2v}^{19}—*Fdd*2 of the crystal the multiplicity $K_M = 4$ indicates that Fe^{3+} ions occupy the sites (16b) with symmetry $G_\alpha = C_1$. To investigate the anisotropic characteristics of the ZFS and CF tensors used in analysis of EPR spectra we adopt the irreducible tensor operators $T_{LM}(\hat{S})$ (*7–9*) since their transformations under rotations of the coordinate system are well tabulated (*9*). To describe the EPR spectrum for Fe^{3+} ions in natrolite we use the SH ($S = 5/2$) with symmetry C_i (*10*),

$$\mathcal{H} = \mathcal{H}_z + \mathcal{H}_2 + \mathcal{H}_4 = \mu_B \vec{B} \cdot g \cdot \hat{S} + \sum_{M=-2}^{2} B_{2M} \bar{T}_{2M} + \sum_{M=-4}^{4} B_{4M} \bar{T}_{4M}, \quad [1]$$

where first term represents the Zeeman interaction, B_{LM} are real ZFS parameters (*11*), and $\bar{T}_{LM}$ are the corresponding hermitian combinations of irreducible tensor operators (*12*): $\bar{T}_{L0} = T_{L0}(\hat{S})$, $\bar{T}_{LM} = T_{LM}(\hat{S}) + (-1)^M T_{L-M}(\hat{S})$, and $\bar{T}_{L-M} = i[T_{LM}(\hat{S}) - (-1)^M T_{L-M}(\hat{S})]$. It should be noted that the form of the last two terms in Eq. [1] is equivalent to the expanded form (*8*) of the ZFS Hamiltonians, whereas the operators $\bar{T}_{LM}$ (*11*) belong to the category of the "normalized combinations of spherical tensor (NCST) operators" (*8*) introduced earlier in (*13, 14*); apart from the coefficient $\sqrt{2}$. Consequently the operators $\bar{T}_{LM}$ are equivalent (to within the scaling factor for a given L) to the normalized Stevens (NS) operators of Gaite *at al*., e.g., (*6, 15*); for details see (*16*) and the review (*8*). Explicit transformation formulas for the parameters B_{LM} under coordinate rotations are given for $L = 2, 4, 6$ in (*11, 17*). The rotational invariant for the ZFS tensor of rank L in Eq. [1] is defined (*11*) as the invariant sum

$$S_L = (B_{L0})^2 + 2 \cdot \sum_{M=1}^{L} ((B_{LM})^2 + (B_{L-M})^2). \quad [2]$$

All SH parameters listed in Table 1 were obtained by fitting the spectral angular dependence in the three crystallographic planes (100), (010), and (001) (Fig. 2) using the modified program (*18*). The RMSD between the calculated and experimental line positions was 0.31 mT, which is of the same order of magnitude as the observed linewidths. Four conjugate spectra are related to each other by the operations 1, m_y, m_x, and 2_z of the point symmetry group C_{2v} of the crystal. Considering the inversion invariance of SH the four sets of the SH parameters can be obtained by rotations through the Euler angles (α, β, γ): (0, 0, 0), (0, π, 0), (π, π, 0), and (π, 0, 0), respectively. Parameters B_{LM} in Eq. [1] are related (*11*) to the ES parameters b_k^q (*8, 16*) used in (*4*), e.g., $B_{20} = (2/\sqrt{6})b_2^0$, $B_{22} = (1/3)b_2^2$. To facilitate direct

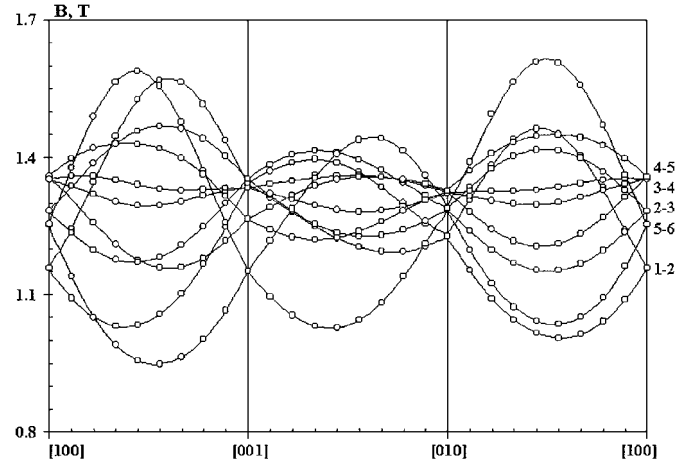

FIG. 2. The angular dependence of EPR spectra of Fe^{3+} in natrolite in the three crystallographic planes (space group *Fdd*2). For convenience, numbers from 1 to 6 in the order of increasing energy denote the states, whereas two numbers denote the transitions between adjacent levels.

TABLE 1

SH Parameters of Fe^{3+} in Natrolite (Space Group *Fdd*2) at 300 K; B_{LM}, b_k^q are in Units of 10^{-4} cm^{-1}; S_4 and $S_4(O_h)$ are in Units of 10^{-8} cm^{-2}; Angles are in Degrees. Value $\varepsilon = \sqrt{\sum_{i=1}^{N} \Delta H_i^2/(N-k)}$ is the RMS Deviation of the Measured and the Computed Resonance Fields with Fit of $k = 20$ Parameters over N Resonance Values Involved

M, q	B_{2M}	b_2^q	B_{4M}	b_4^q	Principal values and axes of tensors	
0	177.3(29)	217.1(83)	−1.9(79)	−7.0(96)		
1	442.7(56)	−2656(54)	−1.1(89)	38.1(33)	$\alpha = 140.3^\circ,\ \beta = 50.16^\circ,\ \gamma = 152.84^\circ$	
−1	223.5(98)	1341.5(88)	−2.3(02)	−73.8(3)		
2	−18.2(41)	−54.7(23)	−1.3(43)	−9.63(1)	$B_{20} = 887.0(8)$	$b_2^0 = 1086.4(5)$
−2	403.4(88)	−1210.4(6)	0.7(90)	−5.6(65)	$B_{22} = 177.4(5)$	$b_2^2 = 532.3(5)$
3			2.5(82)	−219.0(9)	$B_{22}/B_{20} = 0.2$	$b_2^2/b_2^0 = 0.49$
−3			1.0(69)	90.7(08)		
4			0.2(30)	6.9(0)		
−4			2.1(42)	−64.2(6)		
	g − matrix components $g_{ij} = g_{ji}$					
x	2.006(2)	−0.000(2)	−0.000(03)		$\alpha = 196.67^\circ,\ \beta = 14.43^\circ,\ \gamma = 180.43^\circ$	
y		2.0069	−0.000(01)			
z			2.006(3)		$g_{xx} = 2.006(2);\ g_{yy} = 2.006(9);\ g_{zz} = 2.006(3)$	
$S_4 = 47.1;\ S_4(O_h) = 46.1,\ d_4(O_h) = 0.020;\ N = 243;\ \varepsilon = 0.31$ mT						

comparison with other experimental data both sets of parameters are listed in Table 1.

The SH of orthorhombic symmetry D_{2h} was used in (*4*) and SH parameters were found from fitting the spectral angular dependence at 27 GHz taken along the three extreme orientations as follows: $g = 2.003$, $b_2^0 = 1084$, $b_2^2 = 516$, $b_4^0 = 6.6$, $b_4^2 = -65.7$, $b_4^4 = 9.4$ (in units of 10^{-4} cm^{-1}). The orientation of the principal z-axis and the values of the b_2^0, b_2^2 in (*4*) compare well to those of the second rank ZFS tensor in the principal axis system (Table 1). Detailed analysis of the rank 4 ZFS tensor and low-symmetry effects are presented in the next sections.

3. ANALYSIS OF ZFS AND CF TENSORS IN NATROLITE

The values of the diagonal elements of the g-tensor (Table 1) are characteristic for Fe^{3+} at tetrahedral sites (*17*). The ZFS tensor B_4 for Fe^{3+} at tetrahedral sites is mainly determined by its cubic component (*15, 17*). The procedure (*9*) for extracting the maximum invariant component (MIC) of a given symmetry G_s in the tensor B_4 was described in (*6, 11*). The invariant sum for the cubic component, i.e., $G_s = O_h$, of the tensor B_4 is defined (*11*) as

$$S_4(O_h) \equiv \max\ S_4(\alpha, \beta, \gamma; O_h) = \max\left[\sqrt{\frac{7}{12}} \cdot |B_{40}(\alpha, \beta)| + 2 \cdot \sqrt{\frac{5}{24}} \cdot |B_{44}(\alpha, \beta, \gamma)|\right]^2. \quad [3]$$

Equation [3] and the condition $B_{4-4}(\alpha, \beta, \gamma) = 0$, together with the sign equality of B_{40} and B_{44}, determine the system of principal axes ($\xi,\ \eta,\ \zeta$) of the maximum cubic component for the tensor B_4. The coefficient $d_4(O_h) \equiv [S_4 - S_4(O_h)]/S_4$ is the measure of the departure of the tensor B_4 from the exact cubic form for the symmetry O_h.

The values S_4, $S_4(O_h)$, and $d_4(O_h)$ calculated for Fe^{3+} in natrolite are given in Table 1. The cubic axes ($\xi,\ \eta,\ \zeta$) of the tensor B_4 are determined by the Euler angles $\alpha = 62.50^\circ$, $\beta = 63.67^\circ$, $\gamma = 25.65^\circ$ or correspondingly by the direction angles as follows:

B_4	[100]	[010]	[001]
ξ	101.49	56.32	143.90
η	152.65	75.75	67.18
ζ	65.55	37.35	63.67

V_4^{44}	[100]	[010]	[001]
ξ	101.10	55.72	143.47
η	152.42	75.43	67.13
ζ	65.10	38.09	63.21

[4]

To determine the substitution site of Fe^{3+} impurity ions, the natrolite structure was analyzed and the CF tensors V_4^{44} (19) were also calculated using the point charge model at the Al^{3+} and Si^{4+} sites.

The microscopic SH theory and the experimentally established positive cubic parameters in both tetrahedral and octahedral sites for the ^6S-state ions (*17, 19, 20*) indicate that the tensor product $[V_4 \otimes V_4]_4 \equiv V_4^{44}$ dominates the microscopic CF contribution to the ZFS tensor B_4. For this reason, we determine the MIC of cubic symmetry in the axis system ($\xi,\ \eta,\ \zeta$) for the tensor V_4^{44}. The ($\xi,\ \eta,\ \zeta$) system for the tensor V_4^{44} at the Al^{3+} site is determined by Euler angles $\alpha = 61.86^\circ$, $\beta = 63.21^\circ$, $\gamma = 25.81^\circ$ or by the corresponding direction angles given in Eq. [4]. The value of the distortion coefficient $d_4(O_h) = 0.0186$ for the tensor V_4^{44} is close to that obtained for the tensor B_4 (Table 1).

In order to relate the structure of natrolite with the EPR data we also calculated the bond directions in Table 2. This enables the comparison with the principal axes of the MIC of symmetry C_{3i} (*12*) in the tensors B_4 and V_4^{44} (Table 2). The invariant sum

TABLE 2
The Bond Directions in the [AlO_4] Tetrahedron, Principal Axes and Distortion Coefficients of MIC of Symmetry $G_s = C_{3i}$ for the Tensor B_4 (SH) for Fe^{3+} and V_4^{44} (CF) Calculated at Al^{3+} Site in Natrolite; Angles are in Degrees

	Bonds		B_4			V_4^{44}		
[AlO_4]	α°	β°	α°	β°	$d_4(C_3)$	α°	β°	$d_4(C_3)$
Al–O1	118.30	18.68	119.57	18.76	0.0197	119.35	18.45	0.0032
Al–O2	181.83	122.04	179.61	120.00	0.0163	179.05	120.14	0.0119
Al–O3	44.86	115.91	45.26	115.81	0.0135	44.58	115.33	0.0186
Al–O4	290.28	93.60	292.90	90.62	0.0059	292.28	91.31	0.0162

for $G_s = C_{3i}$ is (*12*)

$$S_4(C_{3i}) = \max\{S_4(\alpha, \beta; C_{3i})\} = \max\{(B_{40}(\alpha, \beta))^2 + 2 \cdot [(B_{43}(\alpha, \beta))^2 + (B_{4-3}(\alpha, \beta))^2]\}. \quad [5]$$

For both tensors B_4 and V_4^{44} the principal trigonal axes of MIC of symmetry C_{3i} are practically coincident with the Al–O bond directions in the [AlO_4] tetrahedron (Table 2). This indicates that Fe^{3+} substitute for Al^{3+} in natrolite. The slight modification of nearest environment can be established from the fact that the orientations characterized by the smallest value of $d_4(C_{3i})$ correspond to different bonds for the CF and SH tensors, i.e., Al–O1 for V_4^{44} and Al–O4 for B_4, respectively (Table 2). Close values of the cubic distortion coefficients $d_4(O_h)$ for B_4 and V_4^{44} (see above) additionally demonstrate that $Fe^{3+} \rightarrow Al^{3+}$ substitution induces a small distortion of the coordination tetrahedron.

4. INVARIANTS OF ZFS TENSOR B_4 FOR Fe^{3+} IN OCTAHEDRAL AND TETRAHEDRAL SITES

Octahedral sites exhibit distinctly larger values of S_4 (Table 3), which is consistent with the stronger crystal field strength in

TABLE 3
Invariants of the Rank 4 ZFS Tensors for Fe^{3+} at Tetrahedral and Octahedral Oxygen-Coordinated Sites in Crystals

Crystal	Complex	S_4 (10^{-8} cm^{-2})	a^* (10^{-4} cm^{-1})	Ref.
$YAlO_3$, YAP	[AlO_6]	4735	377[1]	*27*
Mg_2SiO_4, forsterite	[Mg(1)O_6]	1825	234	*31*
$AlSi_2O_4$, kyanite	[Al(2)O_6]	1774	243	*29*
$AlSi_2O_5$, kyanite	[Al(1)O_6]	1508	224	*29*
MgO	[MgO_6]	1400	205	*26*
$Li_2Ge_7O_{15}$, LGO	[Ge(1)O_6]	1329	200	*17*
$Y_3Al_5O_{12}$, YAG	[AlO_6]	1266	195	*28*
$LiAl(SiO_3)_2$, spodumene	[AlO_6]	466	125	*30*
$CaMg(CO_3)_2$, dolomite	[MgO_6]	448	116	*12*
$KTiOPO_4$, KTP	ST1: [Ti(1)O_6]	426	113	*32*
$KTiOPO_4$, KTP	ST4: [Ti(2)O_6]	387	108	*32*
$CaMg(SiO_3)_2$, diopside	[MgO_6]	374	112	*30*
$KTiOPO_4$, KTP	[Ti(1)O_6]	369	105	*10*
$KTiOPO_4$, KTP	ST3: [Ti(1)O_6]	336	100	*32*
$CaCO_3$, calcite	[CaO_6]	325	99	*12*
$Na_2Zn(SO_4)_2 \cdot 4H_2O$, Zn-astrakhanite	[$ZnO_2(H_2O)_4$]	319	98	*25*
$Na_2Cd(SO_4)_2 \cdot 2H_2O$, Cd-kroehnkite	[$CdO_4(H_2O)_2$]	304	95	*25*
$KTiOPO_4$, KTP	ST2: [Ti(2)O_6]	290	93	*32*
Mg_2SiO_4, forsterite	[Mg(2)O_6]	219	81	*15*
CaO	[CaO_6]	138	64	*26*
Mg_2SiO_4, forsterite	[SiO_4]	128	62	*15*
$Y_3Al_5O_{12}$, YAG	[AlO_4]	80	49	*28*
$NaAlSi_3O_8$, albite	[SiO_4]	63	46	*6*
$Na_2[Al_2Si_3O_{10}] \cdot 2H_2O$, natrolite	[AlO_4]	47	38	This work
$Li_2Ge_7O_{15}$, LGO	[Ge(2)O_4]	46	37	*17*
$Li_2Ge_7O_{15}$, LGO	[Ge(3)O_4]	44	36	*17*
$Li_2Ge_7O_{15}$, LGO	[Ge(4)O_4]	44	36	*17*
SiO_2, quartz	[SiO_4]	43	36	*24*

Note. Invariants a^* defined in (*6, 18*) are related to S_4 as $a^* = \sqrt{30S_4}$.

an octahedral environment as compared with that in a tetrahedral environment. The values of S_4 for octahedral sites vary widely (Table 3). The largest value of S_4 was observed for Fe^{3+} in the perovskite-like structure of $YAlO_3$ with no complex anionic groups surrounding the substitution site. Octahedral environments in Cd-kroehnkite and Zn-astrakhanite are formed by O^{2-} ions belonging to the molecular complexes $[SO_4]$ and H_2O and are characterized by the smallest values of S_4 for octahedra. The next nearest neighborhood of Cd^{2+}, Zn^{2+} in both crystals contains ions S^{6+} with high positive charge. In $KTiOPO_4$ the octahedra $[Ti(1)O_6]$ and $[Ti(2)O_6]$ both share vertices with the tetrahedron $[PO_4]$ of the 5-valent P^{5+}. It can be concluded that the increase in both valency and number of next nearest neighbors at the substitution sites decreases the value of S_4.

The tetrahedral substitution sites for Fe^{3+} at the 3- and 4-valent host ion sites cannot be distinguished by the S_4 value alone. This conclusion emphasizes the necessity to investigate the orientation characteristics of both the ZFS and CF tensors. The value of S_4 is sensitive to the specific role the tetrahedra play in the "global" structure of different crystals. It is seen from Table 3 that Fe^{3+} in the isolated tetrahedra $[AlO_4]$ of YAG and that $[SiO_4]$ in forsterite are characterized by a larger value of S_4 in contrast to those forming the framework structure as in quartz, natrolite, and $Li_2Ge_7O_{15}$.

5. DISCUSSION AND CONCLUSIONS

The tensors B_4 (SH) and V_4^{44} (CF) for Fe^{3+} at the $[AlO_4]$ tetrahedral site in natrolite are found to be mainly dominated by their cubic components, the principal axes (ξ, η, ζ) of which nearly coincide with the bisectors of the bonds Al–O in the $[AlO_4]$ tetrahedron. This result is consistent with the previous data (see, e.g., *15, 17, 21*), suggesting the dominance of the cubic component in the ZFS tensor B_4 for Fe^{3+} in octahedral and tetrahedral sites. Our method allows identification of the coordination complex of Fe^{3+} impurity in structure even in the presence of distortion of the local environment.

The comparison of the ionic radii and the valence of isomorphic ions is widely used for prediction of the substitution scheme (*3*). Similarity in ionic radii dominates the preference for substitution comparing with valence equality. If in the case of $LiCaAlF_6$ (*20*) and $Na_2[Al_2Si_3O_{10}] \cdot 2H_2O$ crystals the substitution $Fe^{3+} \rightarrow Al^{3+}$ can reasonably be explained by the closeness of the ionic radii and valence equality, then the substitution of Gd^{3+} for Ca^{2+}, but not for Al^{3+}, in $LiCaAlF_6$ (*11*) can be explained only by the closeness in the ionic radii: $R(Gd^{3+}) = 0.94$ Å, $R(Ca^{2+}) = 1.04$ Å (*3*). The advantage of the topological approach involved is that each conjugate EPR spectrum may be related to a given coordination complex with a specified orientation. The establishment of such correspondence provides a way to estimate the probability of a nonequivalent formation of complexes of different orientation (dissymetrization (*22*)) taking place on the step-like growing face during crystal growth.

The low symmetry effects in the EPR spectra are discussed in details in (*23*). In the cases of monoclinic and triclinic symmetry, the extreme points in spectral angular dependence of different transitions do not coincide. This is a consequence of the noncoincidence of the principal axes of the 2-rank tensors g and B_2 as well as of the principal axes of MIC of the dominant symmetry of tensor B_4. Table 4 lists the extreme values of the resonance magnetic field at $\nu = 36.772$ GHz calculated by using the parameters in Table 1 for the magnetic field directions varied in the vicinity of the principal axes of the tensor B_2. To estimate the contribution of B_4 to this effect we calculated the extreme resonance conditions without the 4-rank ZFS terms, i.e., taking all $B_{4M} = 0$. It is seen from Table 4 that with the nonzero B_4 tensor, the noncoincidence of the extreme points in the EPR spectrum of Fe^{3+} becomes more noticeable. This noncoincidence depends also on the frequency used: at $\nu = 36.7$ GHz the spread of extrema does not exceed 8° but it increases up to 13° at $\nu = 27$ GHz for $\vec{B} \parallel Y$.

It is worthwhile to compare the present results with those for Fe^{3+} in scolecite $CaAl_2Si_3O_{10} \cdot 3H_2O$, the space group C_s^4—$F1d1$ ($a = 18.506$ Å, $b = 18.978$ Å, $c = 6.522$ Å, $\beta = 90°41'$)

TABLE 4

Orientation ($\alpha°$, $\beta°$) of the Extreme Directions and Values of the Resonance Magnetic Field H_{res} (in T) for Different Transitions for Fe^{3+} in Natrolite. The Vicinity of Principal Axes *XYZ* of the B_2 Tensor is Analyzed Using SH Parameters in Table 1 at $\nu = 36.772$ GHz

		$B_4 = 0$			$B_4 \neq 0$		
		$\alpha°$	$\beta°$	H_{res}	$\alpha°$	$\beta°$	H_{res}
$\vec{B} \parallel Z$	$-5/2 \rightarrow -3/2$	140.31	50.13	1.7740	140.81	50.57	1.7765
	$-3/2 \rightarrow -1/2$	140.37	50.13	1.5395	137.06	47.94	1.5378
	$-1/2 \rightarrow +1/2$	140.19	50.25	1.3074	139.31	50.07	1.3068
	$+1/2 \rightarrow +3/2$	140.25	50.19	1.0769	139.12	49.19	1.0795
	$+3/2 \rightarrow +5/2$	140.25	50.15	0.8474	141.25	50.82	0.8454
$\vec{B} \parallel Y$	$-5/2 \rightarrow -3/2$	32.12	69.50	0.9743	30.62	69.32	0.9736
	$-3/2 \rightarrow -1/2$	32.37	69.94	1.1311	35.00	70.82	1.1304
	$-1/2 \rightarrow +1/2$	34.31	71.82	1.2958			
	$+1/2 \rightarrow +3/2$	32.06	69.57	1.4710	37.62	68.63	1.4722
	$+3/2 \rightarrow +5/2$	32.12	69.57	1.6602	32.93	74.82	1.6589
$\vec{B} \parallel X$	$-1/2 \rightarrow +1/2$	101.56	46.93	1.2816	97	48.37	1.2808

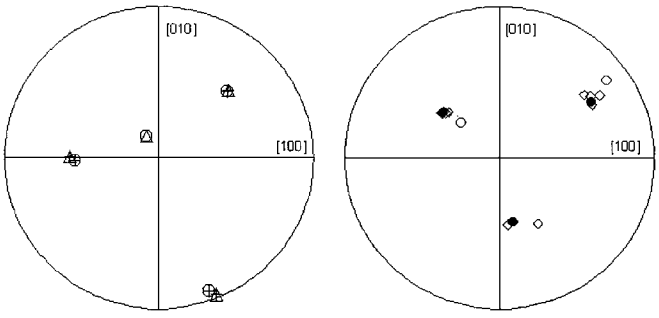

FIG. 3. Stereographic projection of the principal axes, bonds and extreme orientations for Fe^{3+} at Al^{3+} site in natrolite: large circles—Al–O bonds, triangles—principal axes of MIC(C_{3i}) for tensor B_4, full circles—principal axes of tensor B_2, squares—calculated extreme orientations for different transitions, small circles—"magnetic axes" for scolecite.

(*5*). The EPR spectrum multiplicity $K_M = 4$ determined in (*5*) demonstrates that a twinned crystal was studied. The coordinate system of the pseudo-orthorhombic setting used in (*5*) for the magnetic axes directions is convenient for comparison with the data for natrolite ($a = 18.285$ Å, $b = 18.630$ Å, $c = 6.585$ Å). Let us assume that the noncoincidence of the extrema for Fe^{3+} in scolecite is of the same order as that for Fe^{3+} in natrolite (Table 4) and does not exceed 10°–13°. Comparison (Fig. 3) shows that the principal axis directions of the B_2 tensor for Fe^{3+} in natrolite are close to the magnetic axes of the EPR spectrum for Fe^{3+} in scolecite. It can be concluded that the crystal field at the cationic sites within the tetrahedral framework of these zeolites is mainly defined by the structure of the framework by itself, while the mobile extra framework cations serve as the charge compensators perturbing this field.

ACKNOWLEDGMENTS

This work was partially supported by the UGC and the City University of Hong Kong through the research grant SRG 7000768. The careful reading of the manuscript by anonymous referees and their constructive comments were greatly appreciated.

REFERENCES

1. E. Stuckenschmidt, W. Joswig, and W. H. Baur, Refinement of high-order data, separation of internal and external vibrational amplitudes from displacement parameters, *Phys. Chem. Minerals* **19,** 562–570 (1993).

2. I. A. Belitsky, B. A. Fursenko, S. P. Gabuda, O. V. Kholdeev, and Yu. V. Seryotkin, Structural Transformations in Natrolite and Edingtonite, *Phys. Chem. Minerals* **18,** 497–505 (1992).

3. A. Alberti, G. Cruciani, and I. Dauru, Order–disorder in natrolite-group minerals, *Eur. J. Mineral.* **7,** 501–508 (1995).

4. R. Yu. Abdulsabirov, V. M. Vinokurov, M. M. Zaripov, and V. G. Stepanov, Electron paramagnetic resonance of Fe^{3+} ions in natrolite, *Sov. Phys. Solid State* **9,** 541–542 (1967).

5. D. R. Hutton and C. M. Scala, An EPR study of Fe^{3+} in scolecite, *Phys. Status Solidi B* **75,** K167–168 (1976).

6. J. Michoulier and J. M. Gaite, Site assignment of Fe^{3+} in low symmetry crystals: Application to $NaAlSi_3O_8$, *J. Chem. Phys.* **56,** 5205–5213 (1972).

7. D. A. Varshalovich, A. N. Moskalev, and V. K. Khersonskii, "Quantum Theory of Angular Momentum," pp. 1–514, World Scientific, Singapore (1988).

8. C. Rudowicz, Concept of spin Hamiltonian forms of zero-field splitting and electronic Zeeman Hamiltonians and relations between parameters used in EPR, *Magn. Reson. Rev.* **13,** 1–89 (1987); erratum, **13,** 335 (1988).

9. H. A. Buckmaster, R. Chateterjee, and Y. H. Shing, The application of tensor operators in the analysis of EPR and ENDOR spectra, *Phys. Status Solidi A* **13,** 9–50 (1972).

10. G. R. Bulka, V. M. Vinokurov, N. M. Nizamutdinov, and N. M. Khasanova, Pseudosymmetry of spin-Hamiltonian tensor in coordination polyhedral of Fe^{3+} in $KTiOPO_4$ by EPR data, *Sov. Phys. Crystallogr.* **32,** 408–413 (1987).

11. I. I. Antonova, I. N. Nizamutdinov, R. Yu. Abdulsabirov, S. L. Korableva, N. M. Khasanova, A. A. Galeev, V. G. Stepanov, and N. M. Nizamutdinov, EPR of Gd^{3+} in colquiriite single crystal and analysis of the spin Hamiltonian tensors B_4 and B_6, *Appl. Magn. Reson.* **13,** 579–606 (1997).

12. N. M. Khasanova, N. M. Nizamutdinov, V. M. Vinokurov, and G. R. Bulka, Method of maximal invariant components and ESR of Fe^{3+} ions in crystals of calcite and dolomite, *Sov. Phys. Crystallogr.* **33,** 527–533 (1988).

13. D. G. McGavin and W. C. Tennant, Coordinate rotations and relations amongst spin-Hamiltonian parameters in E.P.R. spectroscopy, *Mol. Phys.* **55,** 953–966 (1985).

14. J. A. Tuszynski, H. A. Buckmaster, R. Chatterjee, and J. M. Boteler, Point-group discrimination using the *c*-axis angular variation of the EPR fine structure spectra for S-state ions, *J. Magn. Reson.* **63,** 241–254 (1985).

15. J. M. Gaite and S. S. Hafner, Environment of Fe^{3+} at the M_2 and Si sites of forsterite obtained from EPR, *J. Chem. Phys.* **80,** 2747–2751 (1984).

16. C. Rudowicz, Transformation relations for the conventional O_k^q and normalized O_k^q Stevens operator equivalents with $k = 1$ to 6 and $-k < q < +k$, *J. Physics C* **18,** 1415–1430 (1985); erratum, **18,** 3837 (1985).

17. A. A. Galeev, N. M. Khasanova, A. V. Bykov, G. R. Bulka, V. M. Vinokurov, and N. M. Nizamutdinov, Quadratic crystal field tensors and spin Hamiltonian tensors of Fe^{3+} in $Li_2Ge_7O_{15}$ above and below the phase transition temperature, *Appl. Magn. Reson.* **11,** 61–86 (1996).

18. G. Bacquet, J. Dugas, C. Escribe, J. M. Gaite, and J. Michoulier, Comparative electron paramagnetic resonance study of Fe^{3+} and Gd^{3+} ions in monoclinic zirconia, *J. Phys. C* **7,** 1551–1563 (1974).

19. V. M. Vinokurov, A. R. Al Soufi, A. A. Galeev, N. M. Khasanova, G. R. Bulka, and N. M. Nizamutdinov, Topology of spin Hamiltonian and crystal field tensors for Mn^{2+} in $ZnSeO_4 \cdot 6H_2O$ crystals, *Appl. Magn. Reson.* **7,** 323–337 (1994).

20. N. M. Nizamutdinov, N. M. Khasanova, I. I. Antonova, R. Yu. Abdulsabirov, S. L. Korableva, A. A. Galeev, and V. G. Stepanov, The analysis of spin Hamiltonian and crystal field tensors for Fe^{3+} in crystals of $LiCaAlF_6$ and $LiSrAlF_6$, *Appl. Magn. Reson.* **15,** 145–154 (1998).

21. C. Rudowicz, Derivation of spin Hamiltonian by tensor algebra in perturbation theory, *Acta Phys. Polon. A* **43,** 551–563 (1973).

22. G. R. Bulka, V. M. Vinokurov, N. M. Nizamutdinov, and N. M. Khasanova, Dissymmetrization of crystals: Theory and experiment, *Phys. Chem. Minerals* **6,** 283–293 (1980).

23. J. R. Pilbrow and M. R. Lowrey, Low-symmetry effects in electron paramagnetic resonance, *Rep. Prog. Phys.* **43,** 435–492 (1980).

24. M. J. Mombourquette, W. C. Tennant, and J. A. Weil, ESR study of Fe^{3+} in α-quartz: A reexamination of so-called I center, *J. Chem. Phys.* **85,** 68–79 (1986).

25. N. M. Khasanova, "Invariant Methods of Analysis of Spin Hamiltonian Tensors, EPR Spectra and Coordination Polyhedra in Structure of Doped Crystals" [in Russian], thesis. Kazan University (1990).

26. S. A. Al'tshuler and B. M. Kozyrev, "Electron Paramagnetic Resonance in Compounds of Transition Elements," 2nd ed., Wiley, New York (1974).

27. N. M. Nizamutdinov, N. M. Khasanova, A. A. Galeev, G. R. Bulka, V. M. Vinokurov, V. A. Akkerman, and G. A. Ermakov, Topology of index surface and maximum invariant components of tensors of spin Hamiltonian of Fe^{3+} and Gd^{3+} ions in $YAlO_3$ crystals, *Sov. Phys. Crystallogr.* **34,** 536–541 (1989).

28. V. A. Akkerman, G. R. Bulka, D. I. Vainshtein, V. M. Vinokurov, A. A. Galeev, V. M. Garmash, G. A. Ermakov, A. A. Markelov, N. M. Nizamutdinov, and N. M. Khasanova, Photostimulated and thermally stimulated charge transfer between impurity ions and intrinsic defects in $Y_3Al_5O_{12}$, *Sov. Phys. Solid State*. **34,** 398–402 (1992).

29. J. M. Gaite, H. Rager, and Y. Dusausoy, Localization of Fe^{3+} impurities in kyanite by EPR, *Appl. Magn. Reson.* **21,** 39–48 (2001).

30. J. M. Gaite and J. Michoulier, Electron paramagnetic resonance of Fe^{3+} in diopside and spodumene, *Chem. Phys*. **59,** 488–494 (1973).

31. J. M. Gaite and H. Rager, Electron paramagnetic resonance study of Fe^{3+} at M_1 position in forsterite, *J. Phys. Condens. Matter.* **9,** 10033–10039 (1997).

32. J. M. Gaite, Electron paramagnetic resonance study of paramagnetic defect centres Fe^{3+} and Cr^{3+} in $KTiOPO_4$, *J. Phys. Condens. Matter.* **3,** 7877–7886 (1991).